In situ XAFS study at the Zr *K*-edge for SiO_2/ZrO_2 nano-sol

Jin-Ho Choy,* Joo-Byoung Yoon and Joo-Hyoung Park

National Nanohybrid Materials Laboratory, School of Chemistry and Molecular Engineering, Seoul National University, Seoul 151-747, Korea.
Email:jhchoy@plaza.snu.ac.kr

The structural characterisation of SiO_2/ZrO_2 nano-sol particles, prepared by mixing SiO_2 sol and aqueous solution of $ZrOCl_2$ $8H_2O$, has been carried out by in-situ XAS measurement at the Zr K-edge during condensation reaction. The detailed XANES features at the Zr K-edge of the mixed sol of SiO_2/ZrO_2 are compared with those of other references such as ZrO_2, $ZrOCl_2$ $8H_2O$, $BaZrO_3$, and $ZrSiO_4$, and it becomes obvious that the Zr^{4+} ions are stabilised in an octahedral symmetry. The EXAFS result also indicates that each Zr atom is coordinated with six oxygen ones as the first nearest neighbour, where two oxygen atoms are from the linkage of (Si-O-Zr) at short distance, and four ones are from water molecules at long distance. As the condensation reaction proceeds, it is found that the number of oxygen atoms due to the formation of (Si-O-Zr) bond at short distance and the second neighbour of silicon atoms increase simultaneously. From the above EXAFS and XANES results, the structural and gelating models could be proposed, which is based on the octahedrally coordinated but distorted zirconium species attaching on the SiO_2 sol surface.

Keywords: nano-sol, SiO_2/ZrO_2, sol-gel process

1. Introduction

Sol-gel process is a low-temperature route widely used to obtain multicomponent oxides with a high melting temperature. It also offers unique advantage for the preparation of highly dispersed transparent catalysts, coating materials, and active thin film photocatalysts.(Brinker & Scherrer, 1989) Among various metal oxides, in particular, Zr/Si binary oxides with strong acidic sites have been found to exhibit catalytic activities for dehydrogenation of cyclohexanol(Tseng et al., 1988) and for isomerisation of 1-butene to *cis*- and *trans*-2-butene at 373 K(Yamaguchi et al., 1973). Even though the sol-gel route to silicate glass containing ZrO_2 has been successfully made(Saha & Pramanik, 1993), it is still unclear what processes take place in the sol, especially in a multicomponent system.

In this regard, X-ray absorption spectroscopy (XAS) technique is quite appropriate in investigating the sol-gel process, because XAS can be applied to various systems such as crystalline and amorphous solids, gas, and solution. Moreover, the highly collimated beam from synchrotron radiation makes *in-situ* measurement possible during sol to gel transformation.

In the present study, the structural evolution upon gel transformation from ZrO_2/SiO_2 binary oxide sol has been carefully studied by means of *in-situ* Zr K-edge XAS. The coordination geometry around Zr was probed by XANES (X-ray absorption near edge structure) spectroscopy and EXAFS (extended X-ray absorption fine structure) curve-fitting.

2. Experimental

2.1 SiO_2/ZrO_2 Sol Preparation

The SiO_2 sol was prepared by mixing silicon tetraethoxide, 2 *N* HCl, and ethanol with a ratio of 13.6 ml/3.0 ml/3.8 ml and then the resulting translucent slurry was aged for 1.5 hours at room temperature. In order to prepare ZrO_2 sol solution, zirconium oxychloride hydrate, $ZrOCl_2$ $8H_2O$, was hydrolysed by adding 1 N HCl and ethanol with a rate of HCl / C_2H_5OH / $ZrOCl_2$ $8H_2O$ = 30 ml / 25 ml / 1.97 g, and then the resulting translucent slurry was aged to a clear sol solution with continuous stirring for 5 hours at room temperature. Resulting SiO_2 sol and ZrO_2 one were mixed with a molar ratio of Si/Zr = 10 and the mixture was stirred for 30 minutes at room temperature. The EXAFS measurements for SiO_2/ZrO_2 sol and ZrO_2 one were carried out after the gelation time of 30 min, 3 hours, and 24 hours, respectively. It was confirmed that the sol-gel transformation was completed after 24 hours. As the reference compounds for XAS, ZrO_2 and $ZrOCl_2 \cdot 8H_2O$ from Aldrich were used without any further treatment.

2.2 EXAFS Measurement and Data Analysis

X-ray absorption measurements were carried out with synchrotron radiation by using the EXAFS facilities installed at the beam line 10B in Photon Factory, High Energy Accelerator Research Organization (KEK, Tsukuba). The ring was operated at 2.5 GeV with 350~ 400 mA positron current. A Si(311) channel-cut monochrometer was used where the energy resolution is ~2 eV at the Zr K-edge (17999 eV) for a beam height of ~1 mm.(Nomura & Koyama, 1993) The Zr K-edge absorption data were collected in transmission mode at room temperature using polyethylene solution-cell with a thickness of 1 cm. Absorbance was measured using ionisation chamber filled with N_2(50%) + Ar(50%) and Ar(100%) for incident and transmitted beams, respectively. Only one scan with two second per point (total point = 400) was employed since the sol-gel reaction proceeds slowly. The energy of each spectrum was calibrated from the energy scale of each metal spectrum.

For the XANES and EXAFS data analyses, the inherent background in the data was removed by fitting a polynomial to the pre-edge region and extrapolating it through the entire spectrum, from which it was subtracted. The absorbance $\mu(E)$ was normalised to an edge jump of unity for comparing the XANES features directly with one another. The normalised $\chi(E)$ was then expressed as $\chi(E) = \{\mu(E) - \mu_0(E)\} / \mu_0(E)$. The resulting EXAFS spectra were Fourier-transformed in the range of $2.9 \le k \le 12.6$ Å^{-1} with a Hanning window function of $dk = 0.5$Å^{-1}. In order to determine the structural parameters, a non-linear least-squares curve fitting was performed in the region $0.5 \le R \le 3.5$ Å using the UWXAFS2 code (Stern et al., 1995). The backscattering amplitude, $F_i(k)$, the total phase shift, $\phi_i(k)$, and the photoelectron mean free path, $\lambda(k)$, have been theoretically calculated by a curved wave *ab-initio* EXAFS code FEFF6.(Rehr et al., 1995)

In the course of non-linear least-squares curve fitting between experimental spectrum and theoretical one, the structural parameters such as bond distance (R_i), Debye-Waller factor (σ_i^2), coordination number (N_i) and threshold energy difference (ΔE_0) were optimised as variables. The amplitude reduction factor (S_0^2) of 0.9 for (Zr-O) bond was obtained from ZrO_2 and was also used for Zr-Si pair.

3. Result and Discussion

1.1 EXAFS of SiO_2/ZrO_2 sol

The k^3-weighted EXAFS spectra and their Fourier transforms (FT) for the SiO_2/ZrO_2 sols are shown in Fig. 1 and 2, respectively, depending on ageing time. The first and second peaks within 2.2 Å can be assigned to the backscattering due to the oxygen neighbours, and the third peak around 2.9 Å can be attributed to the Zr-(Si or Zr) neighbour. The distinct change could be observed in the first (Zr-O) shell where the first peak increases with respect to the ageing time but the second peak simultaneously decreases. It should be noted that the two oxygen shells with different distance exist in the SiO_2/ZrO_2 sol, which gives rise to a highly diminished amplitude compared to ZrO_2 and $ZrOCl_2•8H_2O$. The curve-fittings for k^3-weighted EXAFS and FT have been carried out to investigate the structural parameters, and their results are summarised in Table 1 and 2.

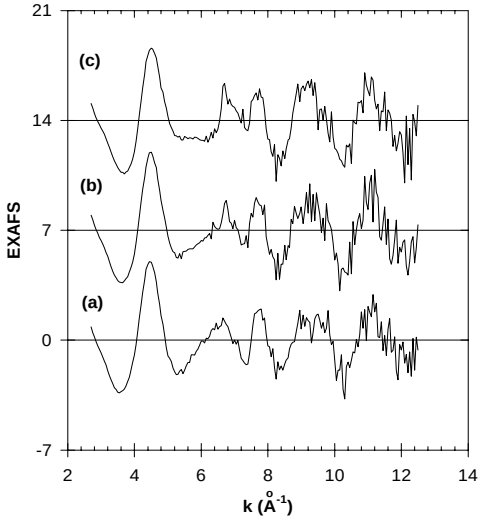

Figure 1.
k^3-weighted EXAFS spectra for SiO_2/ZrO_2 sol depending on ageing time. (a) 30 min, (b) 3 hours, and (c) 24 hours.

According to the EXAFS curve-fitting result for the SiO_2/ZrO_2 sol, the coordination number due to oxygen neighbours was found to be six. And the third peak was fitted by only Si scatterer of which the coordination number increases from two to three depending on the ageing time. The curve-fitting using Zr backscatterer was failed to give physically meaningful parameters. It should be noted that the increase of coordination number from 1.7 to 3.0 due to the first ($Zr-O_1$) pair is consistent with that of the (Zr-Si) pair. Each bond distance is 2.00 Å for $Zr-O_1$ and 2.22 Å for $Zr-O_2$, respectively, and the average bond distance considering the coordination number is ~2.12Å, which is in good agreement with the sum of the ionic radii of octahedrally coordinated Zr^{4+} (0.72Å) and O^{2-} (1.40 Å), suggested by Shannon(Shannon, 1976).

On the other hand, according to the EXAFS of $ZrOCl_2•8H_2O$, the local environment of Zr in an acidic solution was similar to that of solid $ZrOCl_2•8H_2O$ even though the Zr-Zr distance becomes slightly longer.[Table 2] Therefore, it is confirmed that the tetrameric $[Zr_4(OH)_{8+x}(OH_2)_{16-x}]^{(8-x)+}$ ion remains unchanged upon ageing in the present $ZrOCl_2$ solution.

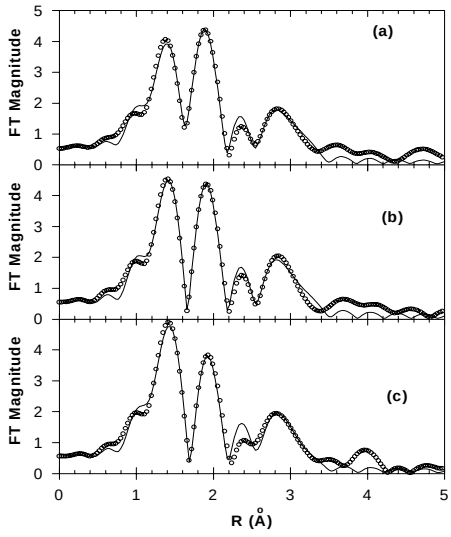

Figure 2.
The Fourier transforms (symbol) and fitting results (solid line) for SiO_2/ZrO_2 sol depending on ageing time. (a) 30min, (b) 3 hours, and (c) 24 hours.

Table 1.
EXAFS fitting results for SiO_2/ZrO_2 sol dependent on the reaction time.

Reaction Time	Bonding type	CN	R (Å)	E_0 (eV)	σ^2($\times10^{-3}$ Å^2)	R factor
	$Zr-O_1$	1.7(4)	1.99(1)	2.9(12)	3.0(10)	
30 min	$Zr-O_2$	4.1(1)	2.22(1)	2.9(12)	9.0(21)	0.016
	Zr-Si	1.9(4)	3.34(2)	6.5(3)	6.1(22)	
	$Zr-O_1$	2.2(2)	1.99(0)	2.8(8)	3.1(9)	
3 hour	$Zr-O_2$	3.9(1)	2.22(1)	2.8(8)	8.5(21)	0.012
	Zr-Si	2.1(4)	3.34(2)	6.9(16)	6.0(15)	
	$Zr-O_1$	2.9(6)	1.99(1)	2.1(13)	4.6(11)	
24 hour	$Zr-O_2$	3.6(1)	2.23(1)	2.1(13)	9.1(31)	0.022
	Zr-Si	2.7(4)	3.33(2)	6.3(22)	8.2(25)	

Table 2.
EXAFS fitting results for $ZrOCl_2•8H_2O$ solution dependent on the reaction time.

Reaction Time	Bonding type	CN	R (Å)	E_0 (eV)	σ^2($\times10^{-3}$ Å^2)	R factor
30 min	Zr-O	7.8(4)	2.20(1)	0.5(8)	10.0(5)	0.062
	Zr-Zr	2.0(3)	3.70(1)		4.3(20)	
3 hour	Zr-O	8.0(4)	2.19(1)	1.0(8)	10.1(6)	0.067
	Zr-Zr	2.0(4)	3.70(2)		3.3(12)	
24 hour	Zr-O	8.2(6)	2.20(1)	0.7(3)	10.0(4)	0.061
	Zr-Zr	2.0(4)	3.70(2)		2.3(10)	
$ZrOCl_2•8H_2O$	Zr-O	8	2.18(1)	0.1(2)	9.8(6)	0.053
	Zr-Zr	2	3.66(2)		2.6(5)	

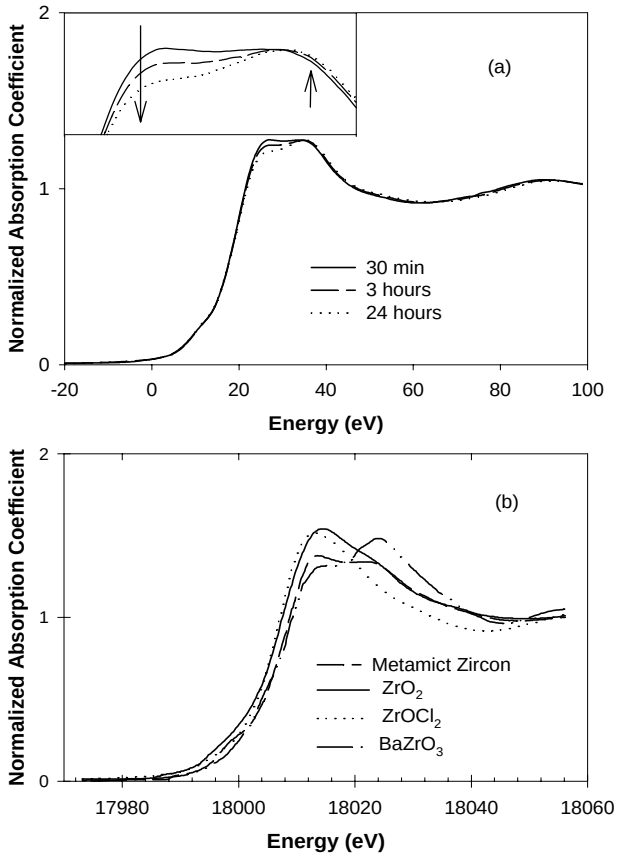

Figure 3.
(a) XANES spectra for SiO_2/ZrO_2 sol depending on ageing time and (b) those for reference compounds.

3.2 XANES of SiO_2/ZrO_2 Sol

Fig. 3 shows the XANES spectra at the Zr K-edge for the SiO_2/ZrO_2 sol with respect to the reaction time. The intensities and energies of shoulder peaks around ~10eV were nearly unchanged. However the peaks at ~20 eV and ~35 eV show systematic changes; the former peak progressively decreases but the latter one increases slightly depending on the ageing time. The shape above 40eV also slightly shifts to a high-energy side upon reaction time.

For the K-edge XANES of transition metal compounds, weak but distinctive absorption peak often appears just before the onset of main absorption one, and it has been designated as the pre-edge due to the electronic transition from inner 1*s* orbital to empty *d* state, as previously described in vanadium compounds (Wong et al., 1984), which is strongly related to the site symmetry of central metal. Often a very intense peak was observed in the compounds with a non-centrosymmetric tetrahedron, where the *d* orbital is mixed with other orbitals of different ℓ-value such as *p* or *s* orbitals. But a very weak pre-edge peak has been also observed in the compounds with centrosymmetric octahedron, which is generally accepted as a quadrupole transition and its intensity is usually only a few percentages compared to a dipole allowed transition. In the present XANES of the SiO_2/ZrO_2 sol the pre-edge peak around ~10 eV appears as a very weak shoulder as shown in Fig. 3, which is similar to that of metamict zircon(Waychunas & Brown, 1990). Therefore, it is certain that the quadrupole transition due to a slight distortion in ZrO_6 octahedron induces such a weak pre-edge peak like in metamict zircon.

The octahedral environment around Zr could also be confirmed in the main edge region. It should be noted that the spectrum after ageing for 24 hours is similar to those of metamict zircon or the other Zr-compounds coordinated with six oxygen atoms but it is different from those of ZrO_2, zircon and $ZrOCl_2 \cdot 8H_2O$ having 7- and 8- coordinated oxygens, respectively, as shown in Fig. 3. (Farges & Brown, 1994, Nakai et al., 1987). On the other hand, the spectral shape beyond 40 eV shifted to a high energy side is consistent with a shortening of average (Zr-O) bond distance as observed in EXAFS result.

3.3 Discussion

In the present study, the reliable gelation model could be proposed on the basis of the above EXAFS and XANES results as follows; As an aqueous solution of $ZrOCl_2 \cdot 8H_2O$ was added into the SiO_2 nano sol one, the positively charged tetrameric $[Zr_4(OH)_{8+x}(OH_2)_{16-x}]^{(8-x)+}$ ions are adsorbed on the surface of negatively charged SiO_2 nano sol, in such a way the surface charge of SiO_2 nano sol becomes positive. As ageing time increases, the formation of (Zr-O-Si) linkage becomes significant due to the condensation between the Zr^{4+} ion on the surface of SiO_2 nano-sol and silanol groups on another SiO_2 one. As a consequence, the numbers of O_1- and Si-neighbours around Zr^{4+} increase, as shown in Table 1, indicating that the gelation of SiO_2/ZrO_2 sol is gradually induced, which is in good agreement with previous small angle X-ray scattering result (Nogami, 1994; Stachs et al., 1995).

This work is financially supported by the Ministry of Science and Technology (NRL program) and partly by BK21 project. We thank Prof. M. Nomura in Photon Factory, High Energy Research Organization for supporting the synchrotron radiation experiment.

References

Brinker, C. J. & G. Scherrer, (1989). Sol-Gel Science; the physics and chemistry of sol-gel processing, p548. San Diego: Academic Press.
Tseng, S. C., Jackson, N. B. & Ekerdt, J. G. (1988). J. Catal. 109, 284.
Yamaguchi, T., Sakai , H. & Tanabe, K. (1973). Chem. Lett. 1017.
Saha, S. K. & Pramanik, P. (1993). J. Non-Crystalline Solids 159, 31.
Nomura, M. & Koyama, A. (1993). KEK Internal, 93-1.
Stern, E. A., Newville, M., Ravel, B., Yacoby, Y. & Haskel, D. (1995). Physica B 208-209, 117.
Rehr, J. J., Zabinsky, S. I. & Albers, R. C. (1992). Physi. Rev. Lett. 69, 3397.
Wong, J., Lytle, F. W., Messemer, R. P. & Maylotte, D. H. (1984). Phys. Rev. B 30, 5596.
Waychunas, G. A. & Brown, G. E. Jr., (1990). Phys. Chem. Minerals 17, 420.
Farges, F., Brown, G. E. Jr., (1994). Am. Mineral. 79, 838.
Nakai, I., Akimoto, J., Kmafuka, M., Miyawaki, R., Sugitani, Y. & Koto, K. (1987). Phys. Chem. Minerals 15, 113.
Shannon, R. D. (1976). Acta Crystallogr. A32, 751.
Nogami, M. (1994). J. Non-Crystalline Solids 178, 320.
Stachs, O., Gerber, Th., Beyer, Y. & Burger, H. (1975). J. Non-Crystalline Solids 180, 197.